Research Square

Preprints are preliminary reports that have not undergone peer review.
They should not be considered conclusive, used to inform clinical practice,
or referenced by the media as validated information.

Pathogenic missense variants in SLC2A1 (GLUT1) misroute to lysosomes in endothelial cells: insights into molecular pathology of GLUT1 deficiency

Sara Lazzari
Casa Sollievo della Sofferenza
Agnese Giovannetti
Agostino Gemelli University Polyclinic
Francesco Petrizzelli
Agostino Gemelli University Polyclinic
Veronica De Paolis
National Research Council
Francesca Matarazzo
National Research Council
Tommaso Biagini
Agostino Gemelli University Polyclinic
Tommaso Mazza
Agostino Gemelli University Polyclinic
Chiara Parisi
chiara.parisi@cnr.it
National Research Council
Viviana Caputo
Sapienza University of Rome

Research Article

Keywords: SLC2A1, GLUT1 DS, missense variants, intracellular mislocalization, lysosomes, trafficking-based phenotyping

Posted Date: April 16th, 2026

DOI: https://doi.org/10.21203/rs.3.rs-9246829/v1

License: This work is licensed under a Creative Commons Attribution 4.0 International License.
Read Full License

Additional Declarations: No competing interests reported.

Version of Record: A version of this preprint was published at Molecular Medicine on July 29th, 2026. See the published version at https://doi.org/10.1186/s10020-026-01584-4.

Abstract

Background

Glucose transporter type 1 (GLUT1), encoded by the *SLC2A1* gene, mediates basal glucose uptake and is essential for brain energy homeostasis. Genetic variants in *SLC2A1* cause GLUT1 deficiency syndrome (GLUT1 DS), a rare neurometabolic disorder characterized by impaired glucose transport across the blood-brain barrier and encompassing a wide and expanding phenotypic spectrum. Although numerous *SLC2A1* missense variants have been identified, their functional interpretation remains challenging and many are currently classified as “variants of uncertain significance”, mainly due to our limited understanding of the underlying molecular mechanisms of pathogenesis. To date, most functional studies have focused on glucose transport activity, while the contribution of altered intracellular trafficking has remained poorly explored.

Methods

Eight *SLC2A1* missense variants were selected and mutants were generated by site-directed mutagenesis of GLUT1-EGFP encoding plasmid. Subcellular localization and trafficking were investigated by using confocal microscopy and quantitative colocalization analysis in human brain endothelial (hCMEC/D3) and HeLa cells, also in response to changes in extracellular glucose availability; protein content in response to autophagy perturbation was evaluated by Western blotting.

Results

We unveiled that four of the selected variants altered GLUT1 distribution and metabolic responsiveness, promoting intracellular retention, with most of them showing marked association to lysosome-related compartments (N34S, R126L and Q283R).

Conclusions

These findings suggest a novel pathogenic mechanism, converging to misrouting to lysosomes, that might represent a shared feature for a subset of GLUT1 missense variants. In this scenario, trafficking-based cellular phenotyping might represent a complementary strategy to conventional transport assays for improving the interpretation of GLUT1 variants and refining genotype-phenotype correlations in the expanding spectrum of *SLC2A1*-related disorders.

BACKGROUND

GLucose Transporter Type 1 (GLUT1), encoded by the *solute carrier family 2 member 1* (*SLC2A1*, MIM *138140) gene, is a facilitated glucose transporter that ensures basal glucose uptake in multiple tissues

and is essential for maintaining systemic energy homeostasis. It is involved in basal glucose uptake in erythrocytes and in the endothelial cells of the blood-brain barrier (BBB), where it plays an essential role in glucose supply to the brain [1]. GLUT1 plasma membrane association is dynamically regulated by trafficking mechanisms responsive to cellular energy status. Once internalized, cytoplasmic GLUT1 can be routed through endosomal compartments, where it may undergo recycling to the plasma membrane or trafficking toward late endosomal/lysosomal pathways, depending on cellular context and metabolic cues [2–3].

Over the years, *SLC2A1* sequence variants have been associated with different disorders, most notably GLUT1 Deficiency Syndrome (GLUT1 DS, MIM #606777 and #612126), a rare genetic neurometabolic disorder caused by impaired glucose transport into the brain, characterized by hypoglycorrhachia, epilepsy, developmental delay, and movement disorders [4–5]. Most cases are sporadic, although autosomal dominant familial cases and, more rarely, recessive familial forms have been described [6–7]. The ketogenic diet is the standard treatment and should be initiated early for optimal outcomes. Approximately 90% of GLUT1 DS patients carry *SLC2A1* mutations resulting in haploinsufficiency representing the main molecular mechanism of pathogenesis [8]. The clinical presentation of *SLC2A1* variants has progressively expanded beyond the classic GLUT1 DS phenotype into a highly heterogeneous continuum characterized by diverse neurological manifestations, variable severity, and differing ages of onset. Accordingly, several distinct neurological disorders and isolated clinical features are currently considered within the expanding spectrum of *SLC2A1*-related conditions [8]. The widespread use of next-generation sequencing (NGS) has further expanded both variant detection and phenotypic recognition. Concurrently, many newly identified variants have been classified as “variants of uncertain significance” (VUS), due to the lack of robust functional tools to assess their pathogenicity. This often necessitates additional clinical and laboratory investigations to support diagnosis, delaying timely therapeutic intervention [9]. This is especially the case of missense variants whose classification, compared to other coding altering variants, is further complicated by our limited comprehension of their biological and functional impact [9].

To date, approximately 550 pathogenic or likely pathogenic variants in *SLC2A1* have been reported in clinical databases (Human Gene Mutation Database, HGMD [10], and ClinVar [11]), including deletions, small insertions and deletions (INDELs), and single nucleotide variants (SNVs). Missense variants, which represent approximately 39% of reported mutations in those databases, are associated with highly heterogeneous phenotypes, including epilepsy, dyskinesias, and ataxia, ranging from mild to severe and occasionally including asymptomatic carriers [8]. In this context, correlations between genotype and phenotype remained elusive [12–13].

To investigate the functional impact of *SLC2A1* variants, different *in silico* and *in vitro* approaches have been employed. *In silico* approaches suggest that missense variants may destabilize GLUT1 structure or alter protein interactions [14–17]. On the other hand, *in vitro* functional assays have been developed to analyze the effect of different types of variants, through the evaluation of the kinetics of glucose transport, primarily in patients’ erythrocytes [18] and *Xenopus* oocyte system [19–20], and, more recently,

through surface quantification assays (METAglut1 [21]). However, while transport assays provide essential information on catalytic activity, they do not capture potential alterations in intracellular routing and spatial distribution that may influence the effective availability of the transporter at the cell surface.

Here, we comparatively examine selected *SLC2A1* missense variants associated with diverse clinical phenotypes and distributed across different structural domains of GLUT1, with the aim of characterizing their subcellular distribution patterns, including their response to changes in extracellular glucose availability. Rather than directly assessing transport kinetics, our study focuses on trafficking-based phenotyping to determine whether distinct variants display differential intracellular routing and compartment association.

For this purpose, we selected eight missense variants aimed at capturing key dimensions of *SLC2A1*-related variability. The panel includes variants located in distinct structural regions of GLUT1, with different levels of clinical and functional evidence, comprising previously reported pathogenic/likely pathogenic variants and one ClinVar VUS (I404V) included as a comparator. Two substitutions affecting the same residue (R223P and R223W) were also included to assess whether alternative amino acid changes at a single position result in divergent trafficking behaviors.

By identifying variant-specific redistribution patterns, this approach provides complementary information to conventional transport-based assays and may improve the interpretation of missense variants within the expanding *SLC2A1*-related clinical spectrum. The selected set should therefore be considered a mechanistically diverse pilot panel rather than a comprehensive representation of *SLC2A1* missense variation.

MATERIALS AND METHODS

SLC2A1 CLONING IN pEGFP-N1 VECTOR AND MUTAGENESIS

To investigate the functional impact of selected GLUT1 missense variants, specific constructs were generated. The human *SLC2A1* gene sequence (NM_006516.4) coding for GLUT1 protein (NP_006507.2) was amplified through PCR from hTERT-RPE1 cells cDNA using the following primers:

SLC2A1 Forward 5’- GAGCAGGAGACCAAACGACGGG – 3’

SLC2A1 Reverse 5’- CACTTGGGAATCAGCCCCCAG – 3’

Fragment was cloned into the Strataclone pSC-A-amp/kan vector and transformed using Strataclone Solo-Pack Competent Cells (Agilent Technologies). Plasmid DNA was isolated using the QIAprep Spin Miniprep Kit (QIAGEN) and subjected to Sanger sequencing using the BigDye Terminator Sequencing Kit v3.1 (Applied Biosystems). Then, the fragment corresponding to the *SLC2A1* coding sequence was subcloned from pSC-A-amp/kan vector to the eukaryotic expression vector pEGFP-N1, in-frame with the EGFP coding sequence at the C-terminal end, using the HindIII (NEB) and SacII (NEB) restriction

enzymes. The DNA construct was transformed into DH5α competent cells, isolated using Plasmid Maxi Kit (QIAGEN), and subjected to Sanger sequencing.

Selected GLUT1 missense variants were introduced in pEGFP-N1-GLUT1 vector by site-directed mutagenesis, using the Phusion Site-Directed Mutagenesis kit (ThermoScientific) with 5'-phosphorylated primers, one of which carries the selected variant. To increase mutagenesis efficiency, Dam-methylated parental plasmid DNA was digested by adding FastDigest DpnI enzyme to the PCR reaction mixture. The DNA construct was transformed into DH5α competent cells, isolated using the Plasmid Maxi Kit (QIAGEN), and Sanger sequenced. All the selected GLUT1 missense variants and the relative primer pairs used for mutagenesis experiments are listed in the **Supplementary Table S1**.

CELL CULTURES

The following cell lines were used for immunofluorescence and/or Western blot experiments. Human Cerebral Microvascular Endothelial Cell Line, hCMEC/D3, was purchased from Cedarlane (cat. #CLU512) and cultured in Endothelial Basal Medium (EBM-2) (Lonza, cat. #190860) supplemented with 10% v/v heat-inactivated fetal bovine serum (FBS) (Life Technologies, cat. #10270-106), 0.1% v/v chemically defined lipid concentrate (Life Technologies, cat. #11905031), 5 µg/ml ascorbic acid (Sigma, cat. #A4544), 1 ng/ml human basic fibroblast growth factor (bFGF) (Sigma, cat. #F0291), 10 mM HEPES (Life Technologies, cat. #15630-080), 1.4 µM hydrocortisone (Sigma, cat. #H0135) and 1% penicillin-streptomycin (Life Technologies, cat. #15140-122). hCMEC/D3 cells were grown on Petri dishes previously coated with a thin layer of collagen I (Collagen Type I, rat tail; Sigma, cat. #08-115), at 37°C in 5% CO_2.

HeLa cells were grown in Dulbecco's modified Eagle's medium (DMEM) (Gibco) supplemented with 10% v/v heat-inactivated fetal bovine serum (FBS), 2 mM L-glutamine (Gibco), and 1% penicillin-streptomycin, at 37°C and 5% CO_2, on uncoated Petri dishes.

For experiments under conditions of glucose deprivation or defined glucose concentrations, Dulbecco's modified Eagle's medium without glucose (Gibco) was used and supplemented, when required, with D-(+)-Glucose solution (Sigma, #G8644).

TRANSFECTION AND IMMUNOFLUORESCENCE EXPERIMENTS

To study the subcellular localization and trafficking behaviour of the selected GLUT1 missense variants, immunofluorescence experiments were performed. hCMEC/D3 cells were seeded at 180,000 cells/well and HeLa cells at 150,000 cells/well in 6-well plates onto 12-mm cover glasses. After 24 h, cells were transfected using Lipofectamine 2000 Transfection Reagent (Invitrogen) with 250 ng of each plasmid in a 2:1 ratio: pEGFP-N1, pEGFP-N1-GLUT1-Wild-Type (WT) / -N34S / -R126L / -R153C / -R223P / -R223W / -Q283R / -I404V / -P485L. Cells were incubated at 37°C in 5% CO_2 for 5 h, then Opti-MEM was replaced by

hCMEC/D3 or HeLa complete medium, and cells were returned to the incubator for 48 h to perform all the experiments under standard culture conditions

To investigate the impact of extracellular glucose availability on GLUT1 trafficking to lysosomes, 24 h after transfection, HeLa cells were subjected to glucose deprivation for 24 h. After glucose deprivation, cells were fixed (t0) or shifted toward different glucose concentrations, i.e. 5 mM, 15 mM, and 25 mM, for 24 h.

To investigate the involvement of the autophagic process, 24 h after transfection, hCMEC/D3 cells were treated with chloroquine (Sigma, #C6628) at a concentration of 100 μM for 2 h or maintained under standard conditions.

For immunofluorescence analysis, cells were fixed with 4% paraformaldehyde for 20 min at room temperature. After permeabilization with 0.1% Triton X-100 for 5 min at room temperature, cells were blocked with 3% bovine serum albumin (BSA) in Phosphate Buffered Saline (PBS) for 30 min. Then, selected primary antibodies were added in 1% BSA buffer and cells were incubated at 37°C for 1 h. To study the subcellular localization of GLUT1 WT and mutant proteins, different primary antibodies were selected to mark specific cellular organelles and structures: Calreticulin Polyclonal antibody (proteintech, cat. #27298-1-AP) to detect endoplasmic reticulum, Golgin-97 (D8P2K) Rabbit mAb (Cell signaling, cat. #13192) for Golgi apparatus, RAB5 (D-11) (Santa Cruz Biotechnology, cat. #sc-46692) for early endosomes, RAB7 Polyclonal Antibody (invitrogen, cat. #PA5-52369) for late endosomes, LAMP1 antibody [H4A3] (abcam, cat. #ab25630) for lysosomes, Monoclonal Pan Cadherin antibody (Sigma-Aldrich, cat. #C1821) for plasma membrane and LC3 (Sigma, cat. #L7543) for autophagosomes. After several washes with 0.2% BSA in PBS, the appropriate fluorescent secondary antibodies were added (Alexa Fluor® 647 AffiniPure Donkey Anti-Rabbit IgG (H + L), Jackson ImmunoResearch, cod. #711-605-152; Rhodamine (TRITC) AffiniPure® Donkey Anti-Rabbit IgG (H + L), Jackson ImmunoResearch, cat. #711-025-152; Rhodamine (TRITC) AffiniPure® Donkey Anti-Mouse IgG (H + L), Jackson ImmunoResearch, cat. #715-025-150) followed by incubation at room temperature for 1 h under gentle agitation. After further several washes with 0.2% BSA in PBS, nuclei were stained with 4',6-diamidino-2-phenylindole (DAPI) (Sigma). Coverslips were extensively rinsed and mounted onto microscope slides using Fluoromount Aqueous Mounting Medium (Sigma).

IMAGES ACQUISITION AND COLOCALIZATION QUANTIFICATION

3D confocal images were sequentially acquired by Olympus' PLAPON 60X OSC2 super-corrected objective confocal apparatus. Sequential 0.5-μm-thick z-stacked sections were imaged through the entire cell profile using a 60 × objective lens and were used to create maximum intensity projections (MIPs) and processed with Fiji (National Institute of Health). All images were acquired with the same laser intensity before the analysis in Fiji. Colocalization of two fluorophores that are aligned with no cross-talk was quantified using Pearson's correlation coefficient (PCC) within the desired areas of the images. Imaging data from the experiments were analyzed using the Coloc 2 plugin of the Fiji

distribution of ImageJ software (http://imagej.net/Coloc_2). Individual areas were selected as regions of interest (ROIs) before applying a mask and running the plugin. After running the plugin, Pearson's R value (no threshold) reported in the ImageJ Log window was recorded for each cell. Values shown represent mean ± sem (30 cells). Statistical significance was determined by an unpaired Student's t-test ($p < 0.01$).

WESTERN BLOT ANALYSIS

To assess whether perturbation of autophagy could affect the steady-state levels of GLUT1 protein, Western blot analysis was performed to quantify GLUT1-EGFP protein in control condition and after chloroquine administration. For this purpose, hCMEC/D3 cells were seeded at 180,000 cells/well in 6-well plates and transfected as previously described. After 24 h of transfection, chloroquine was administered at a concentration of 100 µM for 2 h, then proteins were extracted using RIPA buffer and 100X protease inhibitors (SERVA, cat. #39102.01) for 30 min on ice and centrifuged at 12,000 g for 15 min at 4°C. Proteins were resolved using SDS-PAGE, transferred to nitrocellulose membranes (GVS North America, cat. #1215471), blocked with 5% nonfat dried milk powder (ITW reagents, cat. #A0830) in TBS tween 0,1% for 1 h, and incubated at 4°C overnight with primary antibodies (Purified anti-GFP Epitope Tag Antibody, Biolegend, cat. #902601; Anti-β-Actin–Peroxidase antibody, Sigma-Aldrich, cat. #A3854) followed by incubation with secondary antibodies (Peroxidase AffiniPure® Rabbit Anti-Mouse IgG (H + L), Jackson ImmunoResearch, cat. #315-035-003) for 1 h at RT. Immunocomplexes were detected by chemiluminescence (WesternBright Sirius, Advansta, cat. #K-12043-D10) and analyzed by densitometry using ImageJ. Statistical significance was determined by paired Student's t-test ($p < 0.05$).

RESULTS

Subcellular Localization of WT and Mutant GLUT1-EGFP Proteins in hCMEC/D3 Cells

To investigate variant-associated differences in GLUT1 subcellular localization and trafficking, we selected eight missense variants using criteria aimed at generating a mechanistically diverse comparison set. The panel included variants reported in the literature and/or clinical databases (HGMD, ClinVar) in association with the *SLC2A1*-related phenotype spectrum (N34S, R126L, R153C, R223P, R223W, Q283R, and P485L), together with one missense variant currently reported as VUS in ClinVar and lacking previous functional evidence (I404V), included as a comparator. Variants were chosen to span distinct topological/structural regions of GLUT1 and to capture heterogeneity in prior clinical and experimental support. In addition, R223P and R223W were both included to assess whether different substitutions at the same residue could be associated with similar or divergent trafficking phenotypes. The selected variants should therefore be regarded as a targeted pilot panel rather than as a representative sampling of all *SLC2A1* missense variants. Details of the selected variants are summarized in **Supplementary Table S2**.

We firstly analyzed plasma membrane association of WT and selected GLUT1-EGFP mutants in hCMEC/D3 cells with an antibody that specifically recognizes all the cadherin family members.

Qualitative confocal microscopy showed that GLUT1 WT was predominantly distributed on the plasma membrane, as expected, comparable to the R153C, R223P, R223W and I404V mutants. Conversely, N34S, Q283R, R126L and P485L mutants showed reduced colocalization with the plasma membrane marker and a concomitant increase in intracellular signal intensity (**Fig. 1A; Supplementary Fig. S1A**). Morphologically, N34S and Q283R and to a lesser extent R126L, appeared as rounded, dense intracellular structures, whereas P485L displayed a different distribution pattern characterized by multiple small vesicular structures dispersed throughout the cytoplasm.

Quantitative colocalization analysis between GLUT1-EGFP and cadherins signals performed by using the Pearson's correlation coefficient (PCC) disclosed no statistically significant differences for most mutants compared to the WT protein (mean PCC=0.67). Conversely, P485L displayed substantial lower PCC values (mean PCC=0.36), and a small but significant decrease was observed for Q283R (mean PCC=0.58) (**Fig. 1B; Supplementary Fig. S1B**).

Subcellular Trafficking of WT and Mutant GLUT1-EGFP Proteins in hCMEC/D3 Cells

Confocal microscopy analysis revealed appreciable colocalization of the WT protein with both early and late endosomes. The R153C, I404V, R223P and R223W mutants displayed a subcellular localization pattern comparable to that of the WT across all analyzed markers, i.e. the endoplasmic reticulum (Calreticulin), Golgi apparatus (Golgin-97), early endosomes (RAB5), late endosomes (RAB7), and lysosomes (LAMP1) (**Fig. 2-4**; **Supplementary Fig. S2-S6**).

Conversely, the N34S, Q283R and R126L mutants showed extensive colocalization with the lysosomal marker LAMP1. Of note, the majority of analyzed cells showed a near-complete overlap with LAMP1-positive compartments, particularly in the case of the N34S and Q283R mutants (**Fig. 4A**). Quantitative colocalization analysis of GLUT1-EGFP and LAMP1 signals revealed significantly higher PCC values for N34S (mean PCC=0.76), Q283R (mean PCC=0.76) and R126L (mean PCC=0.64) compared with the WT protein (mean PCC=0.27). (**Fig. 4B; Supplementary Fig. S6B**).

A different localization pattern was observed for the P485L mutant, which formed intracellular structures with a characteristic morphology that colocalized with the Golgi apparatus and early endosomes (**Fig. 2A and Fig. 3A**). PCC values for the P485L mutant were approximately eight-fold higher than those of the WT for the Golgi apparatus marker Golgin-97 (mean PCC of WT=0.09; P485L=0.78) and nearly two-fold higher for the early endosomes' marker RAB5 (mean PCC of WT=0.47; P485L=0.81). Conversely, the N34S, Q283R, and R153C mutants showed PCC values comparable to those of the WT (**Fig. 2B and Fig. 3B**).

Subcellular Localization of WT and Mutant GLUT1-EGFP Proteins in HeLa Cells

To validate our findings in a different cellular context, we performed immunofluorescence experiments in HeLa cells. We analyzed GLUT1 WT and the mutants N34S, Q283R, and P485L, which had shown

significant differences in plasma membrane, early endosomes and lysosomes' localization in hCMEC/D3 cells. The R153C mutant was also included, as its subcellular distribution was comparable to that of the WT.

Confocal microscopy images revealed evident intracellular retention for the N34S, Q283R, and P485L mutants, and a predominant membrane localization for the R153C mutant, similar to the WT, consistent with what was observed in hCMEC/D3 cells (**Supplementary Fig. S7A**).

Quantitative colocalization analysis of GLUT1-EGFP and cadherins signals resulted in a statistically significant reduction for the Q283R and P485L mutants compared with the WT (mean PCC=0.71), albeit with markedly different values (mean PCC: Q283R=0.58; P485L=0.27), consistent with the trend observed in hCMEC/D3 cells (**Supplementary Fig. S7B**).

Similarly, in HeLa cells, intracellular accumulations of the N34S and Q283R GLUT1 mutants overlapped almost completely with LAMP1-positive signals. Quantitative colocalization analysis between GLUT1-EGFP and the lysosomal marker LAMP1 confirmed a significant increased colocalization for the N34S (mean PCC=0.71) and Q283R (mean PCC=0.59) mutants compared with the WT (mean PCC=0.43), whereas the P485L mutant showed a slightly higher PCC value that did not reach statistical significance (mean PCC=0.54; p=0.03) (**Supplementary Fig. S8**).

Colocalization analysis of GLUT1-EGFP and the early endosomes marker RAB5 revealed significantly greater overlap in all tested mutants compared with the WT (**Supplementary Fig. S9A**). Quantitative analysis showed low mean PCC for the WT (mean PCC=0.14), whereas all mutants resulted in significantly higher levels of colocalization, albeit to varying extents. Among them, the P485L mutant displayed the highest increase (mean PCC=0.58), consistent with its behaviour in hCMEC/D3 cells (**Supplementary Fig. S9B**).

Trafficking of WT and Mutant GLUT1-EGFP in HeLa cells Under Different Extracellular Glucose Conditions

We investigated whether extracellular glucose availability differentially affects the lysosomal localization of WT and mutant GLUT1-EGFP proteins (N34S, Q283R, P485L and R153C) in HeLa cells. Confocal microscopy analysis revealed that the shift from glucose deprivation to supplementation, at all tested concentrations (5 mM, 15 mM, 25 mM), resulted in increased colocalization with LAMP1-positive compartments of the WT protein as well as all mutants (**Fig. 5A; Supplementary Fig. S10**).

Quantitative colocalization analysis of GLUT1-EGFP WT and LAMP1-positive compartments showed limited colocalization under glucose deprivation condition (mean PCC=0.16). Glucose supplementation resulted in an approximately four-fold increase in colocalization, with no significant differences among the three tested glucose concentrations. A similar trend was observed for the mutants: GLUT1-EGFP-LAMP1 colocalization increased following glucose administration, generally with comparable responses across all glucose concentrations tested.

However, the magnitude of the relative changes differed among the mutants. The R153C mutant exhibited low colocalization under glucose deprivation, which increased markedly, more than three-fold in terms of PCC, following glucose supplementation, similarly to the WT. In contrast, the N34S, Q283R, and P485L mutants showed substantial colocalization with LAMP1-positive compartments even under glucose deprivation, with significantly higher PCC values compared with the WT in the same condition, and colocalization further increased following glucose supplementation.

The only exception to this trend was observed in the Q283R mutant. The mean PCC value increased from t0 to 5 mM and 15 mM glucose, without significant differences between these conditions, but decreased following exposure to 25 mM glucose, reaching levels comparable to those observed under glucose deprivation (**Fig. 5B-C**). Confocal microscopy analyses showed that, under the 25 mM glucose condition, GLUT1 displayed predominant intracellular localization (**Fig. 5A; Supplementary Fig. S10D**), however, quantitative analysis indicated that it did not fully colocalize with LAMP1-positive compartments.

Involvement of Autophagic Machinery in the Intracellular Localization of mutant GLUT1-EGFP proteins in hCMEC/D3

To investigate whether GLUT1 mutants associate with autophagosome-related compartments, IF analyses were performed in hCMEC/D3 cells by tracing autophagosomes through the LC3 marker, as well as lysosomes. The experiments were carried out on GLUT1 WT, R153C, N34S, Q283R and P485L mutants, under standard conditions and following chloroquine treatment, which increases lysosomal pH and impairs fusion between autophagosomes and lysosomes and is commonly used to perturb autophagy flux [22]. Qualitative analysis of confocal microscopy images revealed that cells transfected with the WT construct displayed punctate LC3 staining under basal conditions, which became more evident following chloroquine treatment, consistent with the expected accumulation of LC3-positive structures upon autolysosomal inhibition. Moreover, chloroquine administration led, in several cells, to the appearance of small GLUT1-EGFP-enriched vesicles partially colocalizing with LC3 puncta. In contrast, the N34S and Q283R mutants showed large LC3-positive puncta, even under basal conditions, which were concentrated in areas enriched in lysosomes and showed extensive colocalization with both LAMP1 and intracellular GLUT1-EGFP-positive structures. Following chloroquine treatment, LC3-positive structures displayed an altered distribution pattern, appearing more diffusely organized around lysosome-enriched regions (**Fig. 6A**).

Moreover, following chloroquine treatment, a fraction of the N34S and Q283R mutant GLUT1 accumulations showed reduced overlap with LAMP1-positive compartments. This was confirmed by quantitative colocalization analysis between GLUT1-EGFP and LAMP1 signals (**Fig. 6A-B**). hCMEC/D3 cells expressing the P485L mutant displayed an LC3 staining pattern characterized by multiple puncta predominantly distributed around lysosome-enriched areas, both under control conditions and following chloroquine treatment. However, under standard culture conditions, P485L intracellular localization showed limited overlap with both LC3 and LAMP1, as reported above. Furthermore, chloroquine

treatment did not alter this distribution pattern, and quantitative analysis of GLUT1-EGFP and LAMP1 colocalization revealed similar mean PCC values (**Fig. 6A-B**).

The R153C mutant behaved similarly to the WT. Under basal conditions, it showed weak and punctate LC3 staining; however, following chloroquine treatment, several cells exhibited a more evident intracellular punctate distribution of GLUT1-EGFP, with some foci partially colocalizing with prominent LC3-positive structures (**Supplementary Fig. S11**).

To assess whether perturbation of autophagy could affect steady-state GLUT1 levels, we performed Western blot analysis to quantify GLUT1-EGFP protein levels in hCMEC/D3 cells transfected with the same constructs under basal conditions and following chloroquine treatment. In cells expressing GLUT1 WT, chloroquine exposure resulted in an increase in GLUT1-EGFP protein levels, indicating sensitivity of GLUT1 WT levels to autolysosomal inhibition. A comparable effect was observed in cells expressing the R153C variant. In contrast, chloroquine treatment did not significantly alter GLUT1-EGFP protein abundance in cells expressing the N34S, Q283R, or P485L mutants **(Fig. 7A-B)**.

DISCUSSION

In this study, we investigated selected GLUT1 missense variants to assess their subcellular localization and trafficking in response to changes in metabolic conditions. These variants localize in different structural domains of the GLUT1 protein, including cytoplasmic (R153C, R223P, R223W, P485L), extracellular (N34S), and transmembrane regions (R126L, Q283R, I404V). The analyzed variants have been reported in the literature and in clinical databases in association with both classic GLUT1 DS and the broader *SLC2A1*-related phenotypic spectrum, characterized by variable clinical severity. The eight missense variants analyzed show different levels of clinical and functional evidence in databases and in the literature. Seven variants are classified as disease-causing mutation (DM) in HGMD and six of these are concurrently classified as pathogenic in ClinVar (N34S, Q283R, R153C, R126L, R223W and P485L). R223P is classified as a risk factor in ClinVar, while I404V is not reported either as a DM variant in HGMD or as a pathogenic/likely pathogenic variant in ClinVar. The number of patients reported in the literature for these variants varies considerably, ranging from single cases to approximately 20–30 patients, and I404V has not been reported in published clinical cases. Hypoglycorrhachia has been documented for several variants, particularly for N34S, R153C, R126L, R223W, and P485L [7, 23–26].

Immunofluorescence analyses were performed in hCMEC/D3 cells, a human brain microvascular endothelial model that recapitulates key properties of the BBB [27], representing a physiologically relevant context for GLUT1-related disorders. GLUT1 WT was predominantly localized at the plasma membrane, with only a few small intracellular vesicles detected in early and late endosomes, consistent with constitutive trafficking through secretory and endosomal compartments reported for GLUT1 [2–3, 28]. A similar distribution was observed for the R153C, R223P, R223W, and I404V mutants with no major alterations across endoplasmic reticulum, Golgi, early or late endosomes, or lysosomes.

For R153C, R223W, and R223P, with previously reported reductions in glucose uptake [12, 20, 29–33], the absence of evident redistribution toward intracellular compartments in our system suggests that their pathogenicity may not primarily involve major alterations in intracellular routing. I404V exhibited a WT-like intracellular distribution profile, with no evident redistribution toward lysosome- or endosome-enriched compartments.

In contrast, N34S, R126L, Q283R, and P485L showed reduced plasma membrane signal and prominent intracellular localization. Among them, N34S, R126L and Q283R had significantly increased colocalization with the lysosomal marker LAMP1, with N34S and Q283R also exhibiting strong association with LC3-positive compartments. R126L, previously shown to reduce membrane expression and glucose uptake in *Xenopus* oocytes and mammalian cells [29, 34–35], displayed increased association with LAMP1-positive compartments, suggesting redistribution toward intracellular compartments that may influence functional availability. For N34S, which has been associated with variable clinical phenotypes (CM052363, HGMD 2025.4 [10]) and reduced glucose uptake in erythrocytes [12, 21, 24, 36], our findings suggest that defective intracellular routing may contribute to its pathogenicity. These trafficking alterations may coexist with structural effects predicted by computational studies, indicating that multiple, non-mutually exclusive mechanisms may underlie the pathogenicity of specific missense variants.

Q283R, for which no previous *in vitro* functional data were available, exhibited one of the most pronounced lysosomal-associated phenotypes, providing the first experimental evidence of a distinct intracellular redistribution phenotype for this variant. P485L displayed a distinct pattern characterized by strong colocalization with Golgi and early endosomal markers and relatively limited association with lysosomes. This phenotype is consistent with previously reported intracellular mislocalization and enhanced interaction with components of the endocytic machinery [37–38]. The divergence between P485L and the lysosome-associated variants further underscores the mechanistic heterogeneity of *SLC2A1* missense mutations.

We replicated immunofluorescence analyses in HeLa cells, which are widely used in functional studies of GLUT1 [28, 39], for GLUT1 WT and for those mutants that showed significant differences in hCMEC/D3 cells. Results in HeLa cells largely confirmed trafficking alterations observed in brain endothelial cells, suggesting that the observed phenotypes are not restricted to a single cellular model, supporting the idea that some of these variants perturb GLUT1 intracellular routing.

Recent reviews have emphasized that GLUT1 trafficking is dynamically integrated with endolysosomal and autophagy-related pathways that respond to cellular metabolic state [40]. Within this framework, the preferential association of selected mutants with LAMP1- and LC3-positive compartments observed in our study supports the view that intracellular distribution of GLUT1 represents a metabolically responsive process rather than a purely degradative endpoint.

Consistent with this concept, our analysis of glucose-dependent redistribution revealed that GLUT1 WT exhibited increased association with LAMP1-positive compartments following glucose supplementation,

indicating glucose-dependent modulation of intracellular compartment association. While R153C retained a similar dynamic profile, N34S, Q283R, and P485L displayed substantial LAMP1 association even under glucose deprivation, suggesting altered responsiveness of intracellular distribution to extracellular glucose availability. The atypical behavior of Q283R at high glucose concentration further indicates that specific missense variants may perturb the coupling between metabolic cues and GLUT1 intracellular routing.

In addition, N34S and Q283R showed a strong association with autolysosome LC3/LAMP1-positive structures, pointing to their aberrant gathering in the autophagic compartments, that was partially reduced upon chloroquine treatment. A defect in the autophagic machinery was then evidenced by analysis of GLUT1-EGFP expression. In fact, while WT and R153C mutant proteins accumulate in response to chloroquine treatment, we did not observe any variation for N34S and Q283R, probably indicating an engulfment of autophagic machinery impeding physiological protein degradation. P485L, which showed limited lysosomal association, was likewise unaffected by chloroquine, consistent with a trafficking alteration occurring upstream of increased LAMP1 association.

These findings suggest that missense variants in *SLC2A1* do not converge on a single pathogenic mechanism but instead differentially affect GLUT1 intracellular distribution patterns and their responsiveness to extracellular glucose conditions. Altered intracellular distribution may represent an additional layer of variability among GLUT1 missense variants. Beyond haploinsufficiency, missense variants may act through additional mechanisms, including altered intracellular trafficking and altered glucose-responsiveness of intracellular distribution.

The progressive increase in reported *SLC2A1* missense variants in ClinVar, many of which remain classified as VUS or with conflicting interpretations, underscores the need for systematic functional characterization to clarify their pathogenic mechanisms. The limited rate of reclassification suggests that many missense variants remain constrained by insufficient functional evidence, creating an ideal scenario for integrating complementary interpretation frameworks [9].

In this context, trafficking-based cellular phenotyping assays may complement conventional transport measurements and contribute to a more accurate interpretation of missense variants, with direct diagnostic and therapeutic implications. A deeper understanding of these mechanisms is critical for the classification of missense variants and for improving genotype-phenotype correlations, with direct implications for timely therapeutic interventions, most notably the initiation of a ketogenic diet, which can significantly improve neurological outcomes. Functional assays based solely on erythrocytes, which lack intracellular membrane systems, may fail to detect variants that primarily disrupt intracellular routing rather than intrinsic transport activity. Phenotypic stratification of missense variants into transport- versus trafficking-defective categories could help prioritize variants for targeted functional validation and open avenues for targeted therapeutic strategies beyond metabolic interventions alone.

Some limitations should be acknowledged. All experiments were performed using overexpression systems with EGFP-tagged constructs. Nevertheless, consistent phenotypes across two independent

cell models support the robustness of the observed alterations.

Moreover, only a subset of reported missense variants was examined. The analyzed variants were selected to provide a structurally and clinically heterogeneous pilot panel, rather than a representative sampling of the full *SLC2A1* missense landscape. Therefore, the relative frequency of the observed trafficking phenotypes should not be generalized to all *SLC2A1* missense variants. Nevertheless, to our knowledge, this is the first study analyzing subcellular localization of such a number of *SLC2A1* missense variants in parallel under identical experimental conditions.

Future studies assessing endogenous models, and a broader panel of variants will help further validate and extend these findings.

CONCLUSIONS

Our study identifies variant-specific intracellular redistribution patterns and altered glucose-responsiveness, supporting trafficking-based phenotyping as complementary evidence for *SLC2A1* missense variants' interpretation.

Abbreviations

GLUT1: Glucose transporter type 1

GLUT1 DS: GLUT1 deficiency syndrome

SLC2A1: solute carrier family 2 member 1

BBB: blood-brain barrier

NGS: next-generation sequencing

VUS: variants of uncertain significance

HGMD: Human Gene Mutation Database,

INDELs: small insertions and deletions

SNVs: single nucleotide variants

FBS: fetal bovine serum

bFGF: basic fibroblast growth factor

DMEM: Dulbecco's modified Eagle's medium

WT: Wild-Type

BSA: bovine serum albumin

PBS: Phosphate Buffered Saline

DAPI: 4',6-diamidino-2-phenylindole

MIP: maximum intensity projection

PCC: Pearson's correlation coefficient

ROI: regions of interest

IF: immunofluorescence

CQ: chloroquine

CTRL: control

DM: disease-causing mutation

Declarations

Ethics approval and consent to participate

Not applicable.

Consent for publication

Not applicable.

Availability of data and materials

All relevant data presented in this study are included in the article and its supplementary information files. Any other data that support the findings discussed here are available from the corresponding authors upon request.

Competing Interests

The authors declare that they have no competing interests.

Funding

This work was supported by EBRI FOE 2023 “Nuove strategie diagnostiche e terapeutiche per le malattie Neurodegenerative e del Neurosviluppo” CUP B53C23009080005 to CP; Sapienza University of Rome (Progetti di Ateneo 2024) to VC.

Authors’ Contributions

SL, AG, TM, CP, VC wrote the original draft and all the authors reviewed and edited the manuscript; SL performed the *in vitro* experiments and related data analysis; VDP, FM validated the experimental data; AG, FP, TB supported the data analysis and curated data presentation; TM, CP, VC conceptualized the study and supervised the project; CP, VC acquired research fundings.

All authors read and approved the final manuscript.

Acknowledgements

Not applicable.

References

1. Scheepers A, Joost H-G, Schürmann A. The glucose transporter families SGLT and GLUT: molecular basis of normal and aberrant function. JPEN J Parenter Enter Nutr. 2004;28:364–71. https://doi.org/10.1177/0148607104028005364.
2. Wu N, Zheng B, Shaywitz A, et al. AMPK-dependent degradation of TXNIP upon energy stress leads to enhanced glucose uptake via GLUT1. Mol Cell. 2013;49:1167–75. https://doi.org/10.1016/j.molcel.2013.01.035.
3. Simonetti B, Guo Q, Giménez-Andrés M, et al. SNX27-Retromer directly binds ESCPE-1 to transfer cargo proteins during endosomal recycling. PLoS Biol. 2022;20:e3001601. https://doi.org/10.1371/journal.pbio.3001601.
4. Seidner G, Alvarez MG, Yeh JI, et al. GLUT-1 deficiency syndrome caused by haploinsufficiency of the blood-brain barrier hexose carrier. Nat Genet. 1998;18:188–91. https://doi.org/10.1038/ng0298-188.
5. De Vivo DC, Trifiletti RR, Jacobson RI, et al. Defective glucose transport across the blood-brain barrier as a cause of persistent hypoglycorrhachia, seizures, and developmental delay. N Engl J Med. 1991;325:703–9. https://doi.org/10.1056/NEJM199109053251006.
6. Klepper J, Scheffer H, Elsaid MF, et al. Autosomal recessive inheritance of GLUT1 deficiency syndrome. Neuropediatrics. 2009;40:207–10. https://doi.org/10.1055/s-0030-1248264.
7. Rotstein M, Engelstad K, Yang H, et al. Glut1 deficiency: inheritance pattern determined by haploinsufficiency. Ann Neurol. 2010;68:955–8. https://doi.org/10.1002/ana.22088.
8. Wang D, Sands T, Tang M, et al. Glucose Transporter Type 1 Deficiency Syndrome. In: GeneReviews® [Internet]. Seattle: University of Washington; 2025.
9. Klepper J. Glut1 Deficiency Syndrome: Novel Pathomechanisms, Current Concepts, and Challenges. J Inherit Metab Dis. 2025;48:e70044. https://doi.org/10.1002/jimd.70044.
10. Stenson PD, Mort M, Ball EV, et al. The Human Gene Mutation Database (HGMD): optimizing its use in a clinical diagnostic or research setting. Hum Genet. 2020;139:1197–207. https://doi.org/10.1007/s00439-020-02199-3.
11. Landrum MJ, Lee JM, Riley GR, et al. ClinVar: public archive of relationships among sequence variation and human phenotype. Nucleic Acids Res. 2014;42:D980–5.

https://doi.org/10.1093/nar/gkt1113.

12. Wang D, Pascual JM, Yang H, et al. Glut-1 deficiency syndrome: clinical, genetic, and therapeutic aspects. Ann Neurol. 2005;57:111–8. https://doi.org/10.1002/ana.20331.
13. Brockmann K. The expanding phenotype of GLUT1-deficiency syndrome. Brain Dev. 2009;31:545–52. https://doi.org/10.1016/j.braindev.2009.02.008.
14. Deng D, Xu C, Sun P, et al. Crystal structure of the human glucose transporter GLUT1. Nature. 2014;510:121–5. https://doi.org/10.1038/nature13306.
15. Park M-S. Molecular Dynamics Simulations of the Human Glucose Transporter GLUT1. PLoS ONE. 2015;10:e0125361. https://doi.org/10.1371/journal.pone.0125361.
16. Galochkina T, Ng Fuk Chong M, Challali L, et al. New insights into GluT1 mechanics during glucose transfer. Sci Rep. 2019;9:998. https://doi.org/10.1038/s41598-018-37367-z.
17. Raja M, Kinne RKH. Mechanistic Insights into Protein Stability and Self-aggregation in GLUT1 Genetic Variants Causing GLUT1-Deficiency Syndrome. J Membr Biol. 2020;253:87–99. https://doi.org/10.1007/s00232-020-00108-3.
18. Klepper J, Garcia-Alvarez M, O'Driscoll KR, et al. Erythrocyte 3-O-methyl-D-glucose uptake assay for diagnosis of glucose-transporter-protein syndrome. J Clin Lab Anal. 1999;13:116–21. https://doi.org/10.1002/(SICI)1098-2825(1999)13:3%3C116::AID-JCLA5%3E3.0.CO;2-C.
19. Wang D, Pascual JM, Iserovich P, et al. Functional studies of threonine 310 mutations in Glut1: T310I is pathogenic, causing Glut1 deficiency. J Biol Chem. 2003;278:49015–21. https://doi.org/10.1074/jbc.M308765200.
20. Zaman SM, Mullen SA, Petrovski S, et al. Development of a rapid functional assay that predicts GLUT1 disease severity. Neurol Genet. 2018;4:e297. https://doi.org/10.1212/NXG.0000000000000297.
21. Mochel F, Gras D, Luton M-P, et al. Prospective Multicenter Validation of a Simple Blood Test for the Diagnosis of Glut1 Deficiency Syndrome. Neurology. 2023;100:e2360–73. https://doi.org/10.1212/WNL.0000000000207296.
22. Klionsky DJ, Abdel-Aziz AK, Abdelfatah S et al. (2021) Guidelines for the use and interpretation of assays for monitoring autophagy (4th edition). Autophagy 17:1–382. https://doi.org/10.1080/15548627.2020.1797280
23. Sánchez-Lijarcio O, Yubero D, Leal F, et al. The clinical and biochemical hallmarks generally associated with GLUT1DS may be caused by defects in genes other than SLC2A1. Clin Genet. 2022;102:40–55. https://doi.org/10.1111/cge.14138.
24. Tayebi N, Leon-Ricardo B, McCall K, et al. Quantitative determination of SLC2A1 variant functional effects in GLUT1 deficiency syndrome. Ann Clin Transl Neurol. 2023;10:787–801. https://doi.org/10.1002/acn3.51767.
25. Mauri A, Duse A, Palm G, et al. Molecular Genetics of GLUT1DS Italian Pediatric Cohort: 10 Novel Disease-Related Variants and Structural Analysis. Int J Mol Sci 23. 2022. https://doi.org/10.3390/ijms232113560.

26. Slaughter L, Vartzelis G, Arthur T. New GLUT-1 mutation in a child with treatment-resistant epilepsy. Epilepsy Res. 2009;84:254–6. https://doi.org/10.1016/j.eplepsyres.2009.01.004.
27. Weksler B, Romero IA, Couraud P-O. The hCMEC/D3 cell line as a model of the human blood brain barrier. Fluids Barriers CNS. 2013;10:16. https://doi.org/10.1186/2045-8118-10-16.
28. Qualls-Histed SJ, Nielsen CP, MacGurn JA. Lysosomal trafficking of the glucose transporter GLUT1 requires sequential regulation by TXNIP and ubiquitin. iScience. 2023;26:106150. https://doi.org/10.1016/j.isci.2023.106150.
29. Pascual JM, Wang D, Yang R, et al. Structural signatures and membrane helix 4 in GLUT1: inferences from human blood-brain glucose transport mutants. J Biol Chem. 2008;283:16732–42. https://doi.org/10.1074/jbc.M801403200.
30. Alter AS, Engelstad K, Hinton VJ, et al. Long-term clinical course of Glut1 deficiency syndrome. J Child Neurol. 2015;30:160–9. https://doi.org/10.1177/0883073814531822.
31. Akman CI, Provenzano F, Wang D, et al. Topography of brain glucose hypometabolism and epileptic network in glucose transporter 1 deficiency. Epilepsy Res. 2015;110:206–15. https://doi.org/10.1016/j.eplepsyres.2014.11.007.
32. Lee EE, Ma J, Sacharidou A, et al. A Protein Kinase C Phosphorylation Motif in GLUT1 Affects Glucose Transport and is Mutated in GLUT1 Deficiency Syndrome. Mol Cell. 2015;58:845–53. https://doi.org/10.1016/j.molcel.2015.04.015.
33. Suls A, Mullen SA, Weber YG, et al. Early-onset absence epilepsy caused by mutations in the glucose transporter GLUT1. Ann Neurol. 2009;66:415–9. https://doi.org/10.1002/ana.21724.
34. Klepper J, Fischbarg J, Vera JC, et al. GLUT1-deficiency: barbiturates potentiate haploinsufficiency in vitro. Pediatr Res. 1999;46:677–83. https://doi.org/10.1203/00006450-199912000-00006.
35. Wong HY, Law PY, Ho YY. Disease-associated Glut1 single amino acid substitute mutations S66F, R126C, and T295M constitute Glut1-deficiency states in vitro. Mol Genet Metab. 2007;90:193–8. https://doi.org/10.1016/j.ymgme.2006.09.002.
36. Klepper J, Scheffer H, Leiendecker B, et al. Seizure control and acceptance of the ketogenic diet in GLUT1 deficiency syndrome: a 2- to 5-year follow-up of 15 children enrolled prospectively. Neuropediatrics. 2005;36:302–8. https://doi.org/10.1055/s-2005-872843.
37. Meyer K, Kirchner M, Uyar B, et al. Mutations in Disordered Regions Can Cause Disease by Creating Dileucine Motifs. Cell. 2018;175:239–e25317. https://doi.org/10.1016/j.cell.2018.08.019.
38. Lacoste J, Haghighi M, Haider S, et al. Pervasive mislocalization of pathogenic coding variants underlying human disorders. Cell. 2024;187:6725–e674113. https://doi.org/10.1016/j.cell.2024.09.003.
39. Yan Q, Lu Y, Zhou L, et al. Mechanistic insights into GLUT1 activation and clustering revealed by super-resolution imaging. Proc Natl Acad Sci U S A. 2018;115:7033–8. https://doi.org/10.1073/pnas.1803859115.
40. Petrosino S, Grumati P. Autophagy and GLUT1 trafficking: an overview of molecular mechanisms. Am J Physiol Cell Physiol. 2026;330:C26–39. https://doi.org/10.1152/ajpcell.00551.2025.

Figures

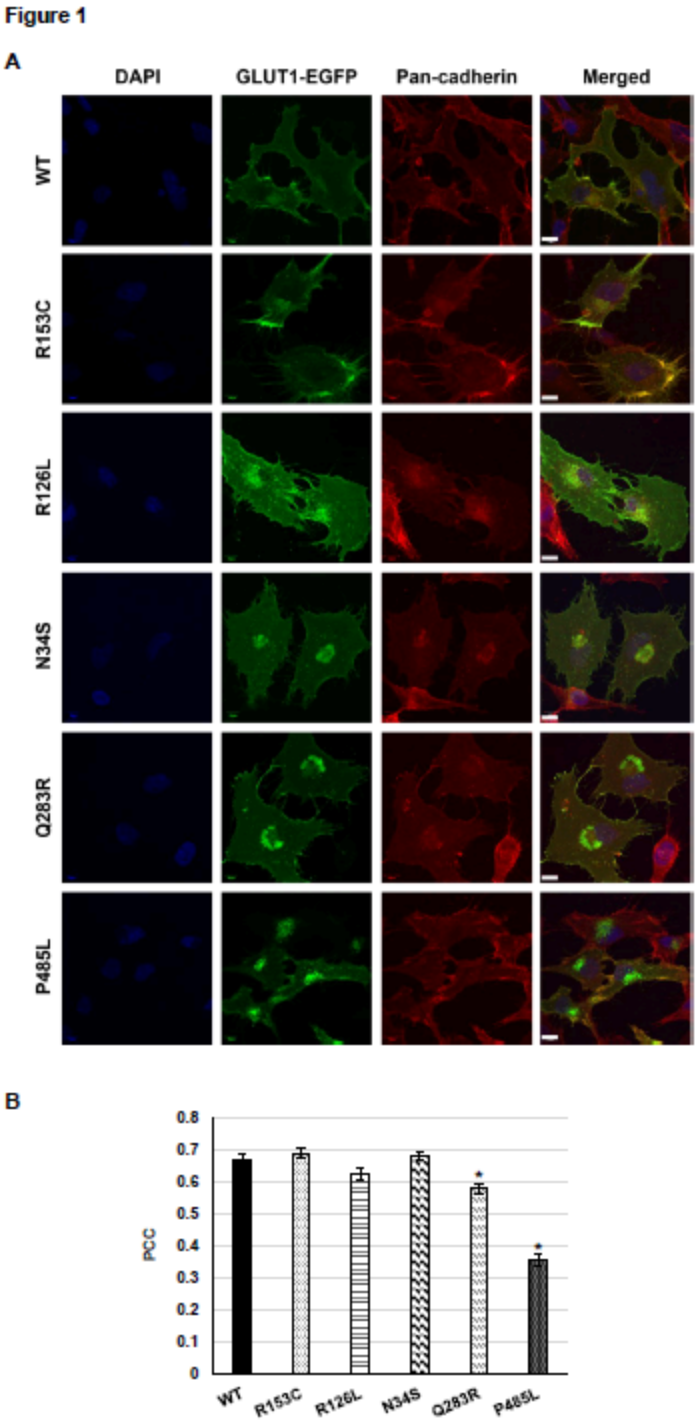


Figure 1

Reduced plasma membrane association for Q283R and P485L mutants in hCMEC/D3 cells. (A) Representative images of immunofluorescence (IF) staining detecting GLUT1-EGFP localization (green) in hCMEC/D3 cells transfected for 48 h with the following constructs: pEGFPN1-GLUT1-WT, pEGFPN1-GLUT1-R153C, pEGFPN1-GLUT1-R126L, pEGFPN1-GLUT1-N34S, pEGFPN1-GLUT1-Q283R, and pEGFPN1-GLUT1-P485L. DAPI (blue) was used to visualize nuclei, cadherins staining (red) detected plasma

membranes. Images are maximum intensity projections of z-stacks. Scale bars 10 µm. **(B)** Quantification of colocalization between GLUT1-EGFP and cadherins' signals. For each experimental condition, Pearson's correlation coefficient (PCC) was calculated within the areas of colocalization using Fiji. PCC was recorded for each cell and reported as mean ± sem on 30 cells. Differences between WT and mutants were analyzed by unpaired Student's t-test. *p<0.01

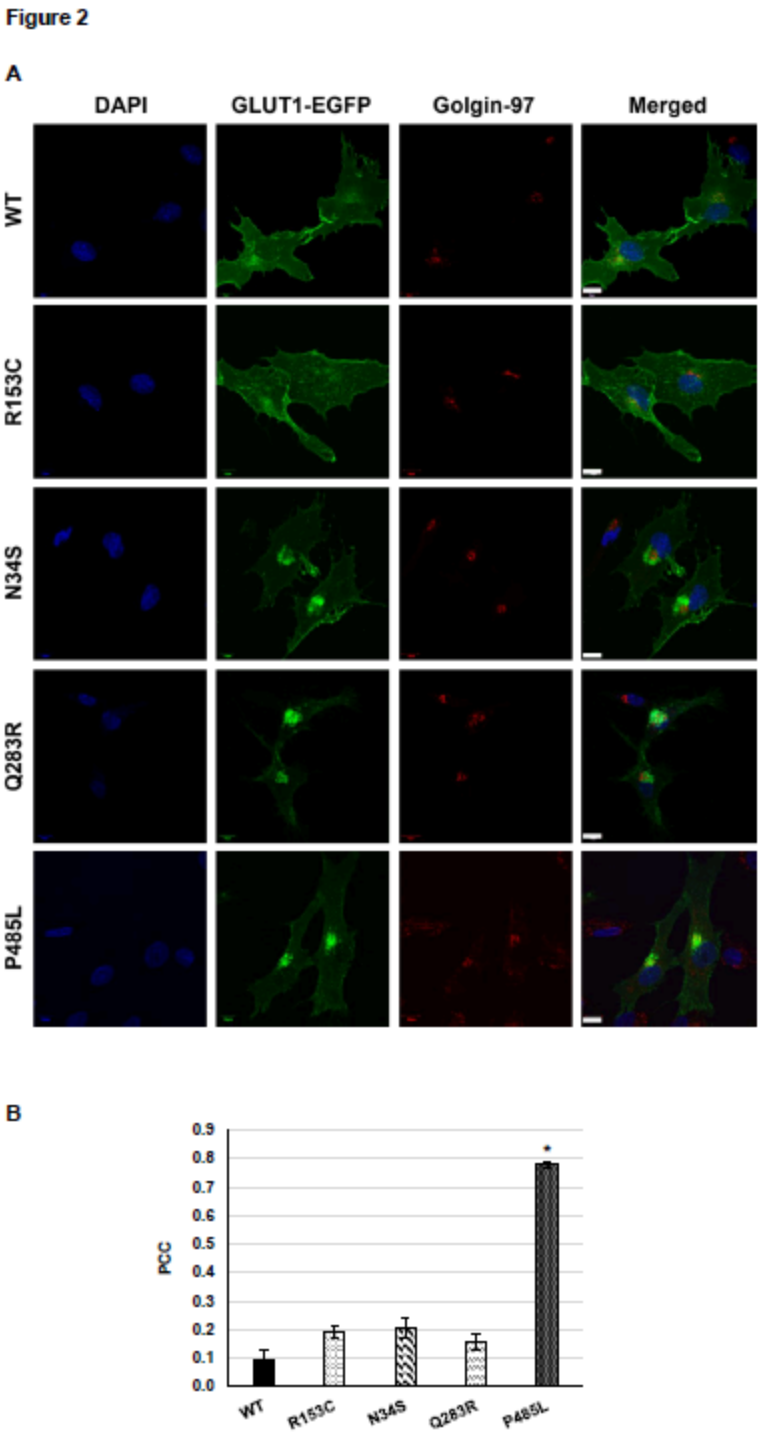


Figure 2

Extensive colocalization of P485L mutant intracellular structures with Golgi apparatus in hCMEC/D3 cells. (A) Representative images of immunofluorescence (IF) staining detecting GLUT1-EGFP

localization (green) in hCMEC/D3 cells transfected with the following constructs: pEGFPN1-GLUT1-WT, pEGFPN1-GLUT1-R153C, pEGFPN1-GLUT1-N34S, pEGFPN1-GLUT1-Q283R, and pEGFPN1-GLUT1-P485L. DAPI (blue) was used to visualize nuclei, Golgin-97 staining (red) detected Golgi apparatus. Images are maximum intensity projections of z-stacks. Scale bars 10 µm. **(B)** Quantification of colocalization between GLUT1-EGFP and Golgin-97 signals. For each experimental condition, Pearson's correlation coefficient (PCC) was calculated within the areas of colocalization using Fiji. PCC was recorded for each cell and reported as mean ± sem on 30 cells. Differences between WT and mutants were analyzed by unpaired Student's t-test. *p<0.01

Figure 3

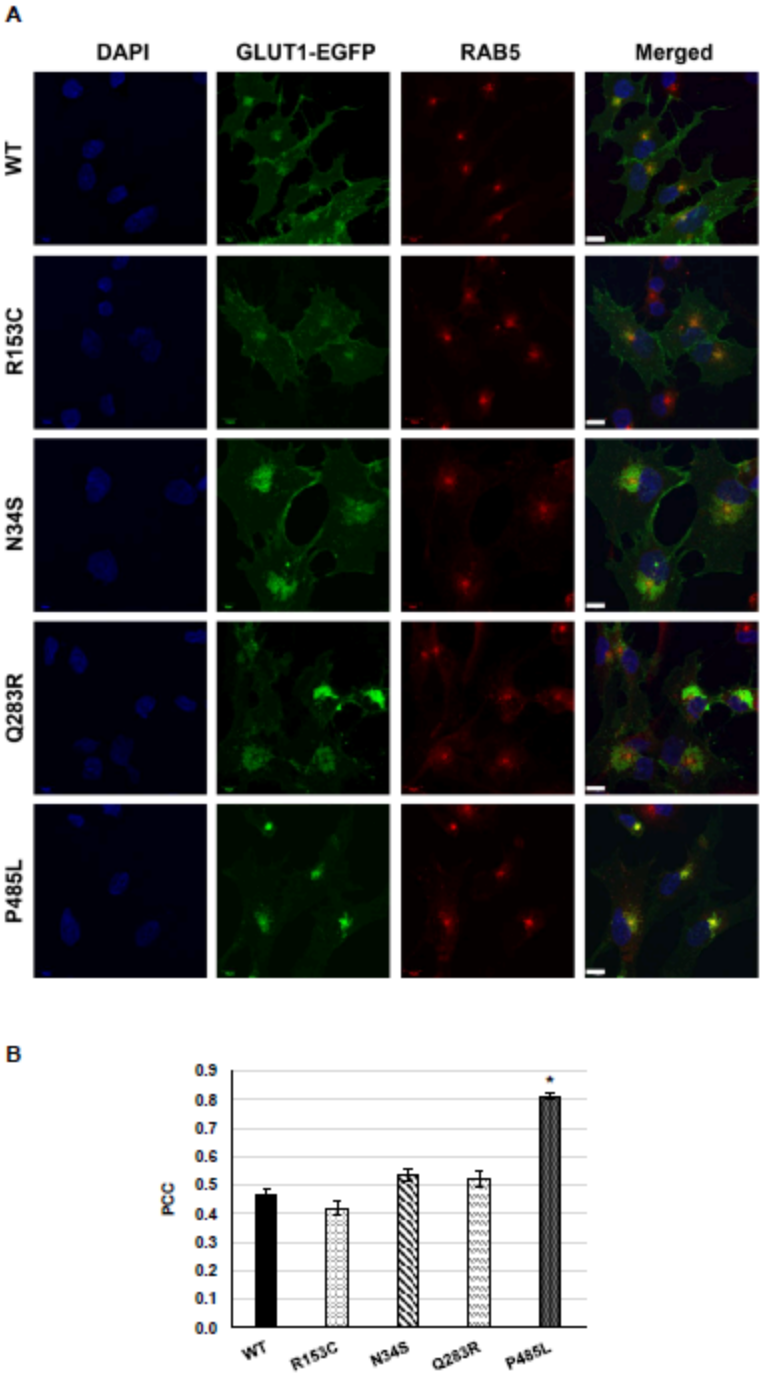


Figure 3

Extensive colocalization of P485L mutant intracellular structures with early endosomes in hCMEC/D3 cells. (A) Representative images of immunofluorescence (IF) staining detecting GLUT1-EGFP localization (green) in hCMEC/D3 cells transfected with the following constructs: pEGFPN1-GLUT1-WT, pEGFPN1-GLUT1-R153C, pEGFPN1-GLUT1-N34S, pEGFPN1-GLUT1-Q283R, and pEGFPN1-GLUT1-P485L. DAPI (blue) was used to visualize nuclei, RAB5 staining (red) detected early endosomes. Images are maximum intensity projections of z-stacks. Scale bars 10 μm. **(B)** Quantification of colocalization between GLUT1-EGFP and RAB5 signals. For each experimental condition, Pearson's correlation coefficient (PCC) was calculated within the areas of colocalization using Fiji. PCC was recorded for each cell and reported as mean ± sem on 30 cells. Differences between WT and mutants were analyzed by unpaired Student's t-test. *$p<0.01$

Figure 4

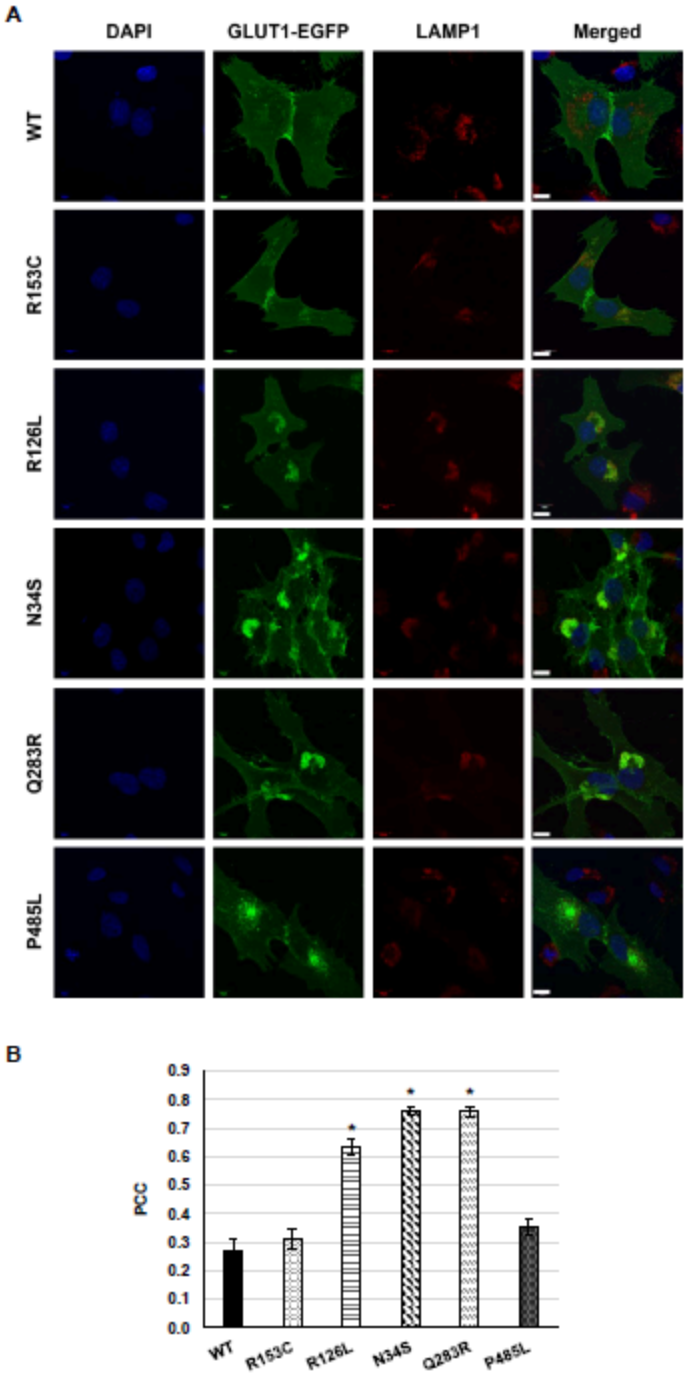


Figure 4

Intracellular structures of N34S, Q283R and R126L mutants in lysosomal compartments in hCMEC/D3 cells. (A) Representative images of immunofluorescence (IF) staining detecting GLUT1-EGFP localization (green) in hCMEC/D3 cells transfected with the following constructs: pEGFPN1-GLUT1-WT, pEGFPN1-GLUT1-R153C, pEGFPN1-GLUT1-R126L, pEGFPN1-GLUT1-N34S, pEGFPN1-GLUT1-Q283R, and pEGFPN1-GLUT1-P485L. DAPI (blue) was used to visualize nuclei, LAMP1 staining (red) detected lysosomes. Images are maximum intensity projections of z-stacks. Scale bars 10 μm. **(B)** Quantification of colocalization between GLUT1-EGFP and LAMP1 signals. For each experimental condition, Pearson's

correlation coefficient (PCC) was calculated within the areas of colocalization using Fiji. PCC was recorded for each cell and reported as mean ± sem on 30 cells. Differences between WT and mutants were analyzed by unpaired Student's t-test. *p<0.01

Figure 5

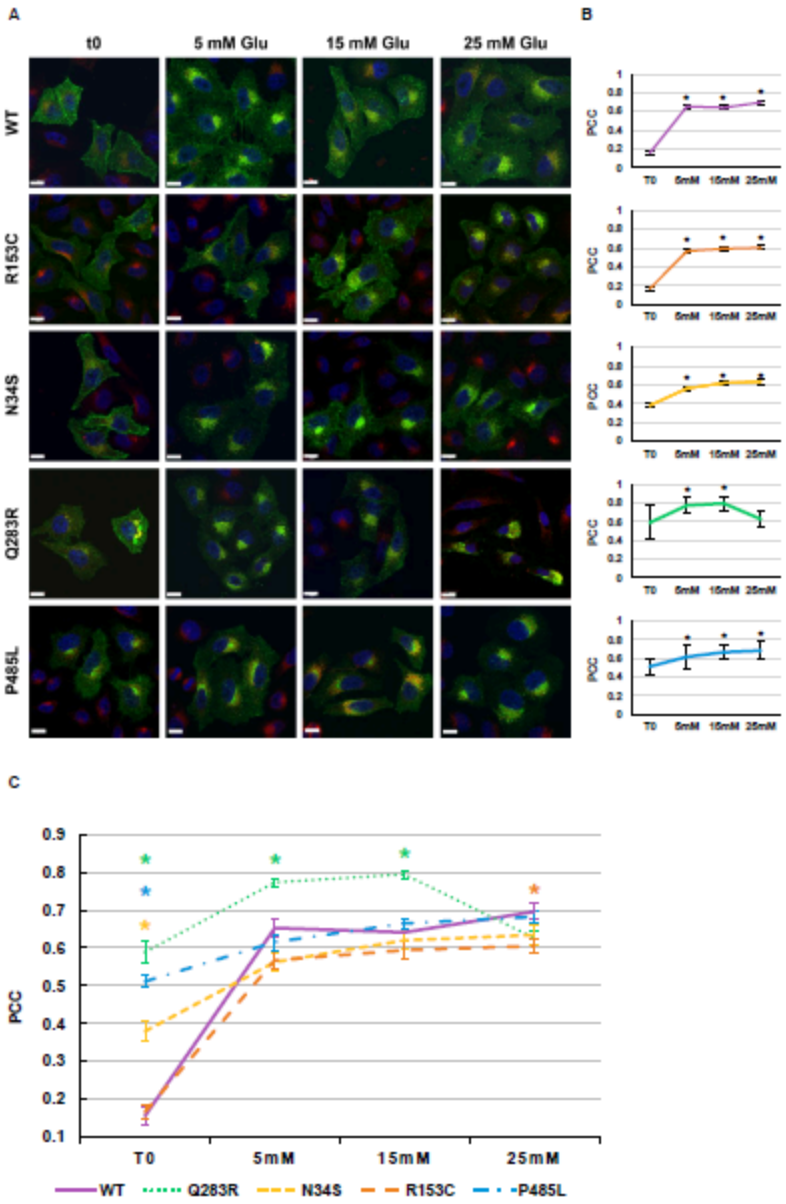


Figure 5

Altered responsiveness of intracellular distribution to extracellular glucose availability in N34S, Q283R and P485L mutants in HeLa cells. (A) Representative images of immunofluorescence (IF) staining detecting GLUT1-EGFP localization (green) in HeLa cells transfected with the following constructs: pEGFPN1-GLUT1-WT, pEGFPN1-GLUT1-R153C, pEGFPN1-GLUT1-N34S, pEGFPN1-GLUT1-Q283R, and pEGFPN1-GLUT1-P485L. Cells were subjected to glucose deprivation for 24 h and then stopped (t0) or

shifted towards different glucose concentrations (5 mM, 15 mM, 25 mM) for 24 h. DAPI (blue) was used to visualize nuclei, and LAMP1 staining (red) detected lysosomes. Images are maximum intensity projections of z-stacks. Only merged images are presented for improved clarity and readability. Scale bars 10 µm. **(B)** Quantification of **A** showing WT and mutants separately in all tested glucose conditions. For each experimental condition, Pearson's correlation coefficient (PCC) was calculated within the areas of colocalization using Fiji. PCC was recorded for each cell and reported as mean ± sem on 30 cells. Differences between t0 and 5mM/15mM/25mM glucose conditions were analyzed by unpaired Student's t-test (*p<0.01). (**C**) Merge of all charts in **B**. Differences between WT and mutants in each experimental condition were analyzed by unpaired Student's t-test (*p<0.01).

Figure 6

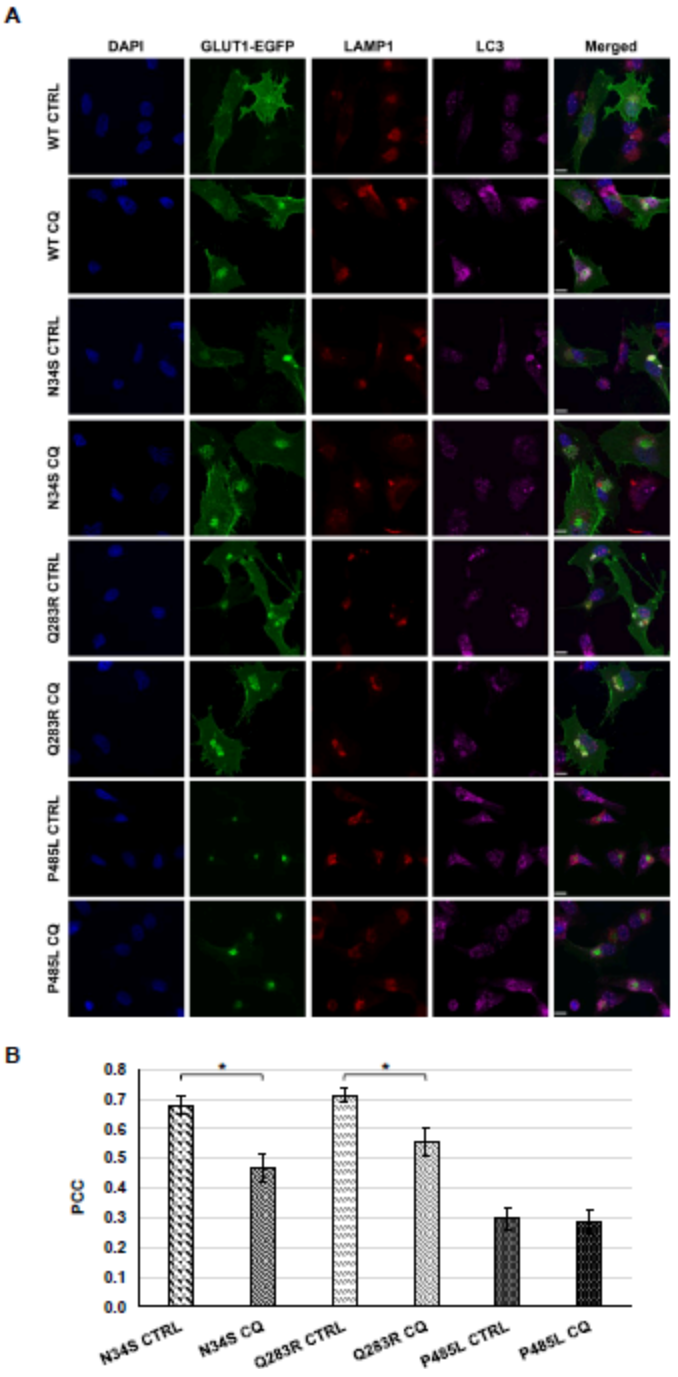


Figure 6

Abnormal enrichment of N34S and Q283R mutants in autophagic compartments. (A) Representative images of immunofluorescence (IF) staining detecting GLUT1-EGFP localization (green) in hCMEC/D3 cells transfected for 24 h with pEGFPN1-GLUT1-WT, pEGFPN1-GLUT1-N34S, pEGFPN1-GLUT1-Q283R, and pEGFPN1-GLUT1-P485L constructs after chloroquine (CQ) treatment for 2 h or under control condition (CTRL). DAPI (blue) was used to visualize nuclei, LAMP1 (red) and LC3 (magenta) stainings detected lysosomes and autophagosomes, respectively. Images are maximum intensity projections of z-stacks. Scale bars 10 µm. **(B)** Quantification of colocalization between GLUT1-EGFP and LAMP1 signals in cells expressing accumulating mutants N34S, Q283R and P485L under control conditions (CTRL) and after chloroquine (CQ) administration. For each experimental condition, Pearson's correlation coefficient (PCC) was calculated within the areas of colocalization using Fiji. PCC was recorded for each cell and reported as mean ± sem on 30 cells. Differences between control condition and chloroquine treatment for each mutant were analyzed by unpaired Student's t-test. *p<0.01

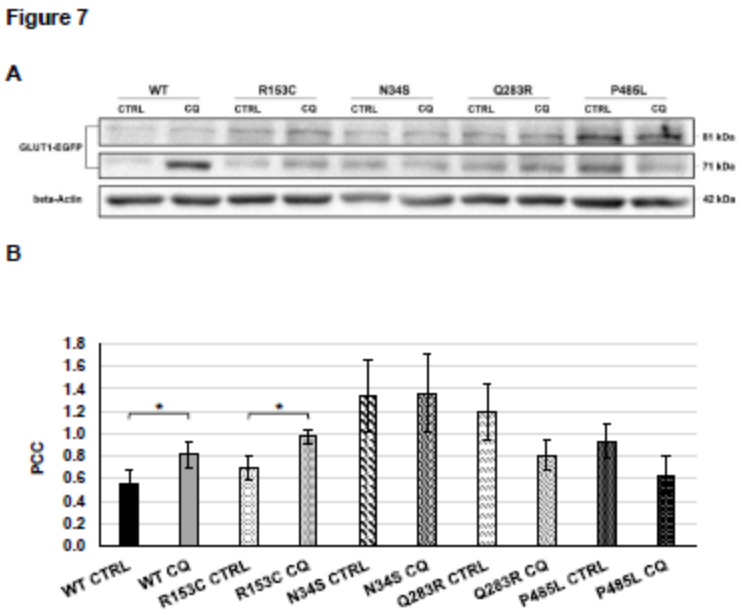


Figure 7

Perturbation of autophagic flux did not affect GLUT1 protein levels in N34S, Q283R and P485L mutants. (A) Representative Western blot of GLUT1-EGFP proteins in hCMEC/D3 cells transfected for 24 h with pEGFPN1-GLUT1-WT, pEGFPN1-GLUT1-N34S, pEGFPN1-GLUT1-Q283R, and pEGFPN1-GLUT1-P485L constructs after chloroquine (CQ) treatment for 2 h or under control condition (CTRL). **(B)** Western blot analysis of **(A)**. The total GLUT1-EGFP protein corresponding to the sum of high (81 kDa) and low (71 kDa) glycosylated bands was normalized on the β-Actin protein level and reported as mean ± sem (n=3 for each experimental group). Differences between control condition and chloroquine treatment for each construct were analyzed by paired Student's t-test. *p<0.05.

Supplementary Files

This is a list of supplementary files associated with this preprint. Click to download.

- SupplementaryMaterial1.pdf
- Supplementarymaterial2.pdf